Simultaneous fingerprinting of multiplex collagen biomarkers in connective tissues by multicolor quantum dots-based peptide probes

Xiangdong Cai [a,b,1], Bo Wang [a,1], Linge Nian [a], Tao Cheng [a], Chunxia Zhang [c], Lu Li [c], Guangrui Zhang [c], Jianxi Xiao [a,*]

[a] *State Key Laboratory of Applied Organic Chemistry, College of Chemistry and Chemical Engineering, Lanzhou University, Lanzhou, 730000, PR China*
[b] *School of Life Sciences, Lanzhou University, Lanzhou, 730000, PR China*
[c] *Tianjin Baogang Rare Earth Research Institute Co., Ltd, PR China*

ARTICLE INFO

ABSTRACT

The accurate detection of multiplex collagen biomarkers is vital for diagnosing and treating various critical diseases such as tumors and fibrosis. Despite the attractive optical properties of quantum dots (QDs), it remains technically challenging to create stable and specific QDs-based probes for multiplex biological imaging. We report for the first time the construction of multi-color QDs-based peptide probes for the simultaneous finger-printing of multiplex collagen biomarkers in connective tissues. A bipeptide system composed of a glutathione (GSH) host peptide and a collagen-targeting guest peptide (CTP) has been developed, yielding CTP-QDs probes that exhibit exceptional luminescence stability when exposed to ultraviolet irradiation and mildly acidic conditions. The versatile bipeptide system allows for facile one-pot synthesis of high-quality multicolor CTP-QDs probes, exhibiting superior selectivity in targeting critical collagen biomarkers including denatured collagen, type I collagen, type II collagen, and type IV collagen. The multicolor CTP-QDs probes have demonstrated remarkable efficacy in simultaneously fingerprinting multiple collagen types in diverse connective tissues, irrespective of their status, whether affected by injury, diseases, or undergoing remodeling processes. The innovative multicolor CTP-QDs probes offer a robust toolkit for the multiplex fingerprinting of the collagen suprafamily, demonstrating significant potential in the diagnosis and treatment of collagen-related diseases.

1. Introduction

Collagen, a superfamily of extracellular matrix proteins with a triple helix structure, is vital for maintaining tissue structure and stability, and it plays a crucial role in mediating physiological processes such as tissue regeneration and wound healing [1–5]. The dysregulation of collagen remodeling has been widely recognized as a key underlying factor contributing to a variety of severe diseases such as tumors and fibrosis [6–9]. The aberrant synthesis and degradation of type I and type IV collagen have been closely implicated in the multifaceted processes of tumor progression, invasion, and metastasis [10–13]. The abnormal accumulation of type I and type IV collagen has been identified in fibrotic lesions, while the excessive degradation of type II collagen is observed in osteogenesis [14–20]. Recent research has highlighted de-natured collagen as a prominent contributor to the progression of tu-mors and other diseases involving collagen dysfunction [21–23].

Therefore, the precise and simultaneous detection of multiplex collagen biomarkers is of utmost importance for the accurate diagnosis and effective treatment of these diseases. Multiplex detection and biomarker fingerprinting have seen significant use in solution. Moreover, the growing interest in tissue-level multiplex detection stems from its pivotal role in disease diagnosis and pathological analysis [24–26].

Fluorescent peptide probes, incorporating widely-used organic dyes like fluorescein and cyanine, have been extensively investigated for the detection of various collagen types [27,28]. The HVWMQAP and KLWVLPK peptide probes, modified with organic dyes, have shown se-lective targeting capabilities for type I collagen and type IV collagen, respectively [29,30]. Furthermore, the peptide probe WYRGRL, labeled with Cy5.5, has been employed to visualize type II collagen in knee joints [31]. A significant recent breakthrough in peptide probe devel-opment has led to the discovery of (GPO)n sequences that selectively target denatured collagen while avoiding binding to intact collagen [32,

33]. However, the tendency of $(GPO)_n$ probes to self-assemble into homotrimers significantly reduces their efficacy in targeting denatured collagen, presenting notable obstacles to their potential clinical utility [34,35]. Moreover, organic dyes are hindered by drawbacks such as photobleaching, limited spectral reusability, and susceptibility to environmental factors, thereby significantly constraining their capacity for simultaneous detection of multiplex biomarkers in complex disease systems.

Quantum dots (QDs) have garnered extensive interest as a prominent choice for multiplex biological imaging, thanks to their remarkable photostability, vibrant color emission, and broad excitation spectra [36, 37]. Various strategies have been investigated for the generation of specific QDs-based probes through the subsequent modification of targeting molecules with pre-synthesized hydrophilic QDs [38]. The coupling strategy, such as 1-(3-Dimethylaminopropyl)-3-ethylcarbodiimide hydrochloride (EDC)/N-Hydroxy succinimide (NHS) chemistry was utilized to crosslink the QDs with a tumor cell-targeting peptide, but the unavoidable self-crosslinking of QDs and peptides frequently leads to precipitation and limits the accessibility of antigen-binding sites [39, 40]. The electrostatic adsorption-based conjugation of negatively charged quantum dots (QDs) with an arginine-rich peptide for nuclei labeling is hampered by the peptides' vulnerability to the external environment, resulting in their detachment from the QDs and subsequent loss of specificity [41]. All previously reported strategies involve additional post-modification steps to create targeting molecules labeled hydrophilic QDs, which frequently result in compromised stability and specificity of the peptide-QDs probes.

We herein for the first time report the construction of multicolor QDs-based peptide probes for simultaneous fingerprinting of multiplex collagen biomarkers in connective tissues. A bipeptide system consisting of a GSH host peptide and a collagen-targeting guest peptide (CTP) has been developed for the one-pot synthesis of highly stable hydrophilic QDs-based probes, demonstrating exceptional specificity towards specific collagen biomarkers, including denatured collagen, type I collagen, type II collagen, and type IV collagen. The multicolor CTP-QDs probes serve as a highly versatile tool for the fingerprinting of multiplex collagen types in a variety of connective tissues, whether affected by injury, disease, or undergoing remodeling processes. The novel multicolor CTP-QDs probes provide a robust toolkit for multiplex collagen fingerprinting, with great potential in the diagnosis and management of collagen-related diseases.

2. Materials and methods

2.1. Synthesis of peptides

All peptides were synthesized in-house by standard Fmoc solid phase peptide synthesis (SPPS) method using rink amide resin. Stepwise couplings of amino acids were performed using Fmoc-amino acids (4 eq.), HOBt (4 eq.), HBTU (4 eq.) and DIEA (6 eq.). Resin was washed by DMF (3 × 10 mL) and DCM (2 × 10 mL) after each coupling step and following Fmoc deprotection with 20% (v/v) piperidine in DMF. Chloranil test was used to check the status of coupling reaction and Fmoc deprotection. For FAM-labeled peptide probes, the mixture of FAM (10 eq.), HOBt (10 eq.), HBTU (10 eq.) and DIEA (16 eq.) in DMF was added to the resin, and incubated for 24 h to conjugate FAM to the *N*-terminal of the peptide. TFA/H$_2$O/TIS (95:2.5:2.5) was applied to treat the resin for 2.5 h to deprotect the side-chain protecting group and take off the peptide. The peptides were harvested by precipitation with cold Et$_2$O. Crude products were collected by re-suspension in cold Et$_2$O, sonication and centrifugation, and were then purified using reverse phase HPLC on a C18 column. The peptides were lyophilized and stored at −20 °C for future use. The identity of the peptides was confirmed by mass spectrometry.

2.2. Synthesis of CTP-QDs probes

All reactions were carried out in oxygen-free water under nitrogen. The synthesis of CTP-QDs was based on the reaction of cadmium chloride with sodium hydrogen telluride (NaHTe). NaHTe was prepared by adding 1 mL NaBH$_4$ (10 mg/mL) dropwise to a powder of Tellurium at 60 °C. Freshly generated NaHTe was bubbled into a solution containing CdCl$_2$ and glutathione (GSH) at pH 11.5 with vigorous stirring. The mixture was heated to 100 °C and then refluxed for 30–120 min. At this point, a solution containing 1 mL collagen-targeting peptides (CTPs) in ultrapure water was injected into the mixture at a rate of 200 μL per minute, and the refluxing process continued for an additional 15 min. The amounts of Cd, Te, GSH and CTPs were 0.1, 0.05, 0.3 and 0.003 mmol, respectively, in a total volume of 30 mL. The as-prepared CTP-QDs was precipitated with an equivalent amount of 2-propanol, and then resuspended in ultrapure water and precipitated with 2-propanol three more times. The pellet of purified CTP-QDs was dried overnight at room temperature in vacuum, and the final product in the powder form could be redissolved in water.

2.3. Physical characterization

The XRD pattern of vacuum-dried CTP-QDs powder was obtained with a D/Max-2400 X-Ray Diffractometer (Ridaku Technologies Inc., Japan). The scanning was performed with Cu Ka radiation (40 kV, 200 mA) at a rate of 0.02°/s within the 2θ range of 10°–80°. The FTIR was obtained with a Fourier Transform Infrared Spectrometer NEXUS 670 (Thermo Nicolet Corporation, Madison, USA). A pellet was formed by grinding 1 mg of CTP-QDs probe powder with 100 mg of anhydrous potassium bromide and compacting the mixture. DLS measurement of CTP-QDs in aqueous solution was acquired with BI-200 S M laser light scattering system (Brookhaven Instruments Corporation). TEM of CTP-QDs was performed on Thermo Scientific™ Talos™ F200C TEM (FEI, Hillsboro, USA).

2.4. Colorimetric measurements

Fluorescent images were captured using a digital camera (Canon SX220 HS) to document the visual representation of CTP-QDs probe solutions, which were illuminated by a UV lamp with 365 nm excitation.

2.5. The absorption and emission spectroscopy

Absorption spectra of CTP-QDs probes were recorded at room temperature on a UV-1750 spectrophotometer (Shimadzu Corporation, Kyoto, Japan). Emission spectra were measured on an RF-6000 fluorescence spectrometer equipped with a Xenon lamp as an excitation source (Shimadzu Corporation, Kyoto, Japan). Fluorescence measurements were conducted from 450 nm to 800 nm with a 1 nm increment per step.

2.6. Tissue staining and imaging

All animal experiments were performed with protocols approved by the ethics committee of College of Chemistry and Chemical Engineering, Lanzhou University (No. G08). All tissues were fixed in a 4% paraformaldehyde solution in 10 mM PBS (pH 7.4) for 1 h and subsequently cryopreserved in Tissue-Tek O.C.T. medium. The tissues were then sectioned to a thickness of 4 μm on glass slides. The tissue slides were air-dried at room temperature, permeabilized by cold methanol at −20 °C for 10 min, and incubated in 10 mM PBS. Each slide was then treated with 0.5 mL blocking solution (10% v/v goat serum in 10 mM PBS), and incubated at room temperature. Solutions of CTP-QDs with a concentration of 0.1 mg/mL and CTP-FAM with a concentration of 20 μM were prepared in 10 mM phosphate buffer (pH 7.4). 100 μL of each probe solution was applied to the tissue slide, and incubated at 4 °C for 6 h

with the tissue slide covered with parafilm. The parafilm was removed, and the solution on the slides was absorbed by bibulous paper. The tissue slides were subjected to three consecutive 5-min washes with 10 mM phosphate buffer. The stained tissue sections were visualized using a Leica DM4000B metallurgical upright microscope (Leica Microsystems Inc., Wetzlar, Germany). For the assessment of luminescence stability of CTP-QDs, the specimens were subjected to continuous illumination for 420 s using light emitted from a 100 W Halogen lamp. Anti-collagen antibodies (1:50 dilution) were used to stain tissues. After blocking, 100 μL antibodies solutions were applied to the tissue sections and incubated at 4 °C for 12 h. The tissue slides were then washed by10 mM phosphate buffer for 5 min three times and probed by FITC labeled goat anti-rabbit IgG (1:500) for 60 min at 37 °C. The tissue slides were subjected to three consecutive 5-min washes with 10 mM phosphate buffer. The stained tissue sections were visualized using a Leica DM4000B metallurgical upright microscope.

3. Results and discussion

3.1. Design of the collagen-targeting peptide modified QDs probes

A bipeptide system comprising glutathione (GSH) as the host peptide and a collagen-targeting peptide (CTP) as the guest peptide has been developed to generate highly stable hydrophilic quantum dots-based probes with exceptional specificity for specific collagen biomarkers (Scheme 1). GSH contributes to the significant stabilization of quantum dots (QDs) by leveraging the electrostatic repulsion effects facilitated by its charged amino acid Glu, while simultaneously establishing coordinative connections through its Cys amino acid. The guest peptide, featuring the shared sequence pattern Cys-Glu-Ahx-CTP, incorporates the selective peptide sequence CTP that specifically targets a particular type of collagen biomarkers [29–31,34]. Moreover, the guest peptide encompasses a coordinative Cys residue for connection to QDs, a negatively charged Glu residue for QDs stabilization via electrostatic repulsion, and aminohexanoic acid (Ahx) as a linker between the Cys-Glu and CTP sequences. Unlike thermally-labile antibodies, CTPs exhibit exceptional thermal stability and can be directly added at the outset of high-temperature reactions, enabling the one-step synthesis of specific hydrophilic QDs and eliminating the need for additional second-step modifications as required by previously reported methods [39,42,43]. Due to its short length, GSH is not expected to interfere with the interaction between the guest peptide and the targeted biomarkers.

The guest peptides offer exceptional flexibility in accommodating different types of collagen-targeting sequences, making them a highly versatile tool for the synthesis of specific peptide probes based on QDs for the detection of multiple collagen biomarkers. Four distinct CTP variants have been designed to specifically detect different forms of collagen: DCTP (CE-Ahx-(GPO)$_8$-NH$_2$) for denatured collagen, ICTP (CE-Ahx-HVWMQAP-NH$_2$) for type I collagen, IICTP (CE-Ahx-WYRGRL-NH$_2$) for type II collagen, and IVCTP (CE-Ahx-KLWVLPK-NH$_2$) for type IV collagen (Table 1).
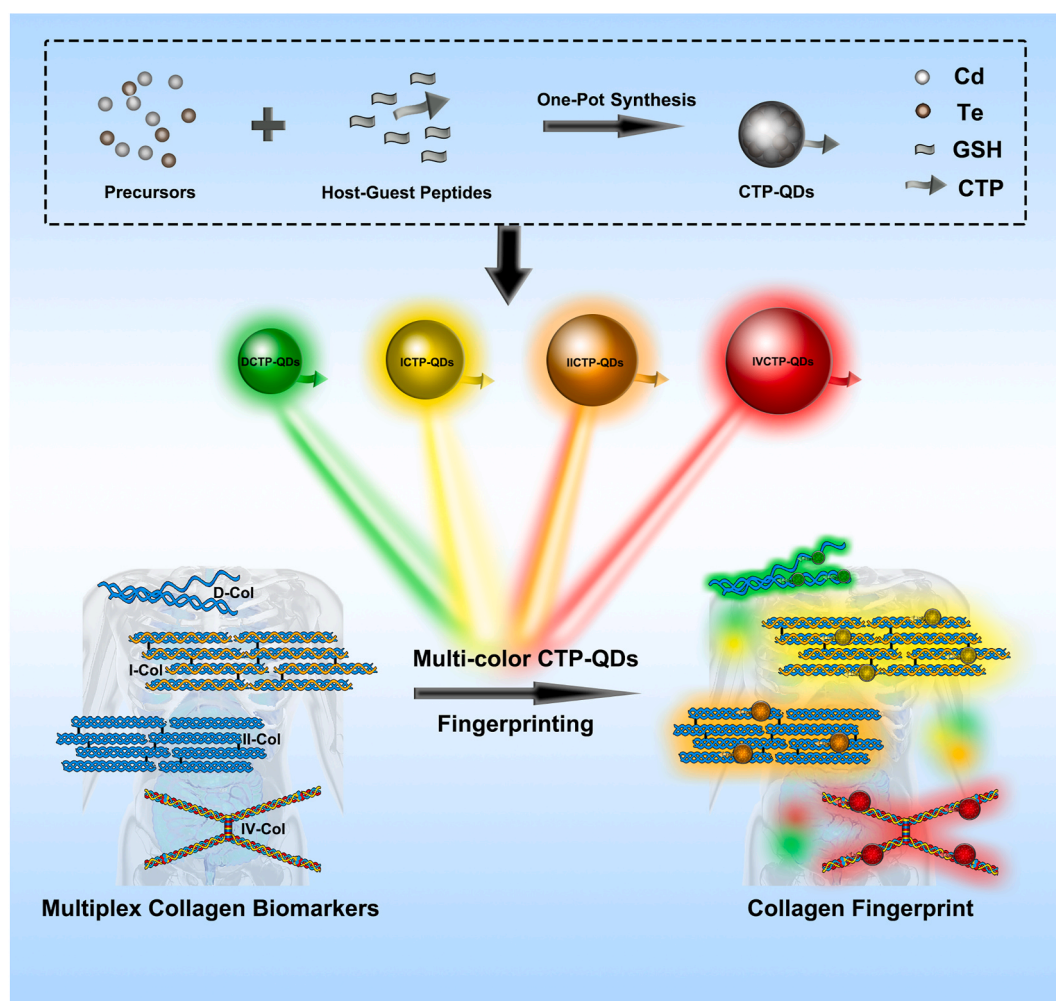
Scheme 1. Schematic illustration of simultaneous fingerprinting of multiplex collagen biomarkers in connective tissues by multicolor quantum dots-based peptide probes.

Table 1

Construction of collagen-targeting peptides. Name, sequence and mass spectroscopy characterization of the peptides and their respective collagen targets.

Name	Sequence	Calculated m/z	Found m/z	Target
DCTP	CE-Ahx-(GPO)$_8$-NH$_2$	2557.8	2557.3	Denatured collagen
ICTP	CE-Ahx-HVWMQAP-NH$_2$	1212.5	1212.3	Type I collagen
IICTP	CE-Ahx-WYRGRL-NH$_2$	1194.4	1194.4	Type II collagen
IVCTP	CE-Ahx-KLWVLPK-NH$_2$	1227.5	1227.5	Type IV collagen

3.2. Synthesis and characterization of multicolor CTP-QDs probes

Four types of CTPs (DCTP, ICTP, IICTP and IVCTP) were successfully synthesized using solid-phase synthetic protocols, and their identity was verified through mass spectrometry analysis (Table 1, Fig. S1). Solutions of 5 mM CdCl$_2$ and 15 mM GSH were prepared in water, and their pH were adjusted to 11.5 by 1 M NaOH. Solutions of NaHTe with a final concentration of 2.5 mM was added to the mixtures, and was heated at 100 °C for 30–120 min under vigorous stirring. Solutions of each type of CTPs (DCTP, ICTP, IICTP and IVCTP) with a final concentration of 0.015 mM were then injected into the mixture, and kept heating at 100 °C for additional 15 min to synthesize DCTP-QDs, ICTP-QDs, IICTP-QDs and IVCTP-QDs, respectively.

Colorimetry, fluorescence spectrometry and UV–vis spectrometry were employed to examine these four CTP modified QDs (CTP-QDs)

prepared at three different incubation time (45 min, 95 min and 135 min) at 100 °C (Fig. 1). DCTP-QDs, ICTP-QDs, IICTP-QDs and IVCTP-QDs with three different colors (green, orange and red) under UV365 light were observed, and their fluorescence emission spectra displayed maximum wavelengths covering a broad range from ~525 nm to ~680 nm (Fig. 1a). The UV–vis spectra of DCTP-QDs, ICTP-QDs, IICTP-QDs and IVCTP-QDs displayed similar broad absorption peaks, indicating that the multicolor CTP-QDs could be excited by the same excitation source (Fig. S2). These findings consistently demonstrated the convenient production of multicolor CTP-QDs by adjusting the incubation time, enabling simultaneous detection of multiple collagen biomarkers using a single readily available excitation source.

All the prepared CTP-QDs with three different colors remained as clear solutions and were analyzed using dynamic light scattering (DLS). The DLS analysis of DCTP-QDs, ICTP-QDs, IICTP-QDs, and IVCTP-QDs consistently demonstrated particle sizes of approximately 3 nm for green-colored CTP-QDs, 4 nm for orange-colored CTP-QDs, and 5 nm for red-colored CTP-QDs, indicating a uniform distribution and excellent dispersion (Fig. S3). Additionally, the gradual increase in particle size, achieved through longer incubation times, corresponded to a redshift in the emission wavelength. The as-prepared red CTP-QDs were selected as examples for further characterization by transmission electron microscopy (TEM) and X-ray diffraction (XRD). The TEM images revealed homogeneously distributed nanoparticles with an average diameter of approximately 5 nm for all CTP-QDs (Fig. 1b). The XRD patterns of red DCTP-QDs, ICTP-QDs, IICTP-QDs, and IVCTP-QDs all showed characteristic peaks at 26° and a broad band at 45°, which corresponded to diffraction planes (111) and overlapped (220) and (311) of zinc blende crystal, respectively (Fig. 1c). These results have constantly
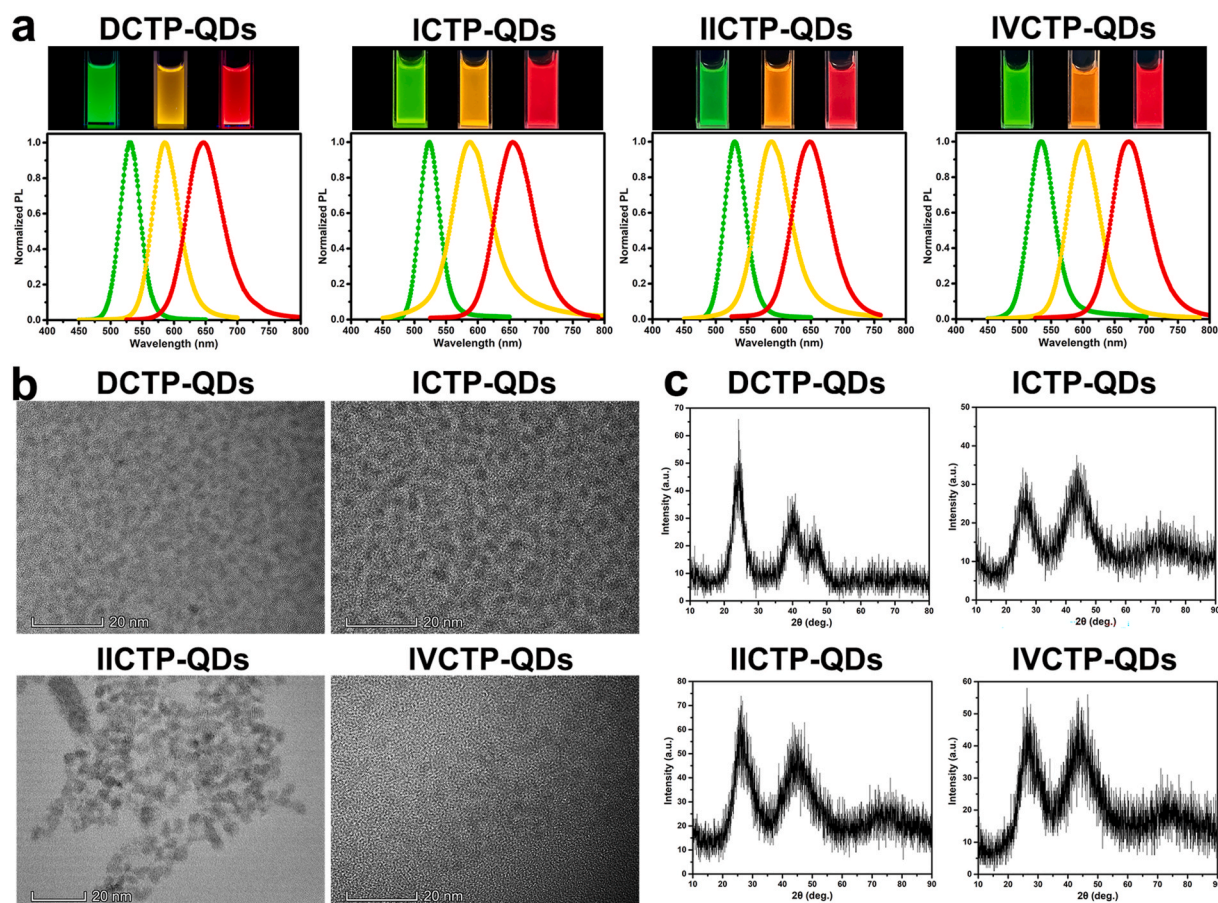

Fig. 1. Characterization of multicolor CTP-QDs probes. a) Photographs and fluorescence spectra of DCTP-QDs, ICTP-QDs, IICTP-QDs and IVCTP-QDs with three different emission wavelengths. The photographs were taken under a UV365 lamp. b) TEM images of DCTP-QDs, ICTP-QDs, IICTP-QDs and IVCTP-QDs. Scale bar = 20 nm. c) XRD patterns of DCTP-QDs, ICTP-QDs, IICTP-QDs and IVCTP-QDs.

demonstrated the formation of high-quality multicolor CTP-QDs with the same crystal type and uniform size.

3.3. Targeting specificity of the CTP-QDs probes

The targeting specificity of DCTP-QDs probes was investigated using fluorescence microscopy (Fig. 2). The DCTP-QDs and DCTP-FAM were prepared under two conditions: equilibrated at 4 °C or heated to 85 °C for 10 min immediately prior to staining tail tissues. The fluorescence micrograph of SDS-treated tail tissues but not the normal tail tissues stained with both preheated DCTP-QDs and preheated DCTP-FAM showed strong green fluorescence, indicating that DCTP-QDs and DCTP-FAM specifically targeted denatured collagen in SDS-treated tail tissues (Fig. 2a–e and 2g). Notably, the fluorescence micrograph of SDS-treated tail tissues stained with unheated DCTP-QDs, but not unheated DCTP-FAM, exhibited intense green fluorescence, indicating that the unheated DCTP-QDs probe retained the collagen-targeting peptide in the single-stranded conformation necessary for binding to denatured collagen (Fig. 2e–h). The inability of unheated DCTP-FAM to bind to denatured collagen was consistent with previous findings that DCTP-FAM tends to adopt a triple helical structure at lower temperatures, thereby hindering its interaction with denatured collagen [27].

The single-stranded stability of both DCTP-QDs and DCTP-FAM probes was assessed by monitoring the real-time fluorescence intensity at 525 nm after subjecting them to heating at 85 °C for 20 min (Fig. S4). The fluorescence intensity of the DCTP-FAM probe rapidly decreased,

exhibiting a 60% reduction within 300 s, suggesting the fast formation of a triple helix structure. In contrast, the DCTP-QDs probe maintained a high fluorescence intensity, indicating its stable single-stranded conformation. The results demonstrated that the larger size of QDs nanoparticles, compared to FAM, effectively inhibited the formation of the triple helix conformation of CTP, while maintaining its binding ability with denatured collagen.

The targeting specificity of DCTP-QDs towards denatured collagen was assessed through binding experiments. Wells of a 96-well plate were coated with thermally denatured type I collagen (Dn-collagen), BSA, trypsin, pepsin, lysozyme, and glycogen. DCTP-QDs probes were added to the wells, and unbound probes were subsequently removed. The strong fluorescence observed in wells coated with denatured collagen, along with negligible fluorescence in wells coated with BSA, trypsin, pepsin, lysozyme, and glycogen, confirms the specific binding affinity of DCTP-QDs probes to denatured collagen and their minimal binding to other biomolecules (Fig. 2i).

The DCTP-QDs probes were employed to assess denatured collagen under various conditions including heat treatment, exposure to denaturants, and UV irradiation. The wells of a 96-well plate were coated with collagen treated under these various conditions, and DCTP-QDs probes were subsequently added for analysis. The fluorescence intensities observed in the wells coated with collagen pre-treated at different temperatures (4 °C, 30 °C, 40 °C, and 60 °C) for 30 min were 100, 750, 4500, and 7500, respectively, indicating minimal denaturation below 30 °C and significant denaturation above 40 °C (Fig. 2j). The
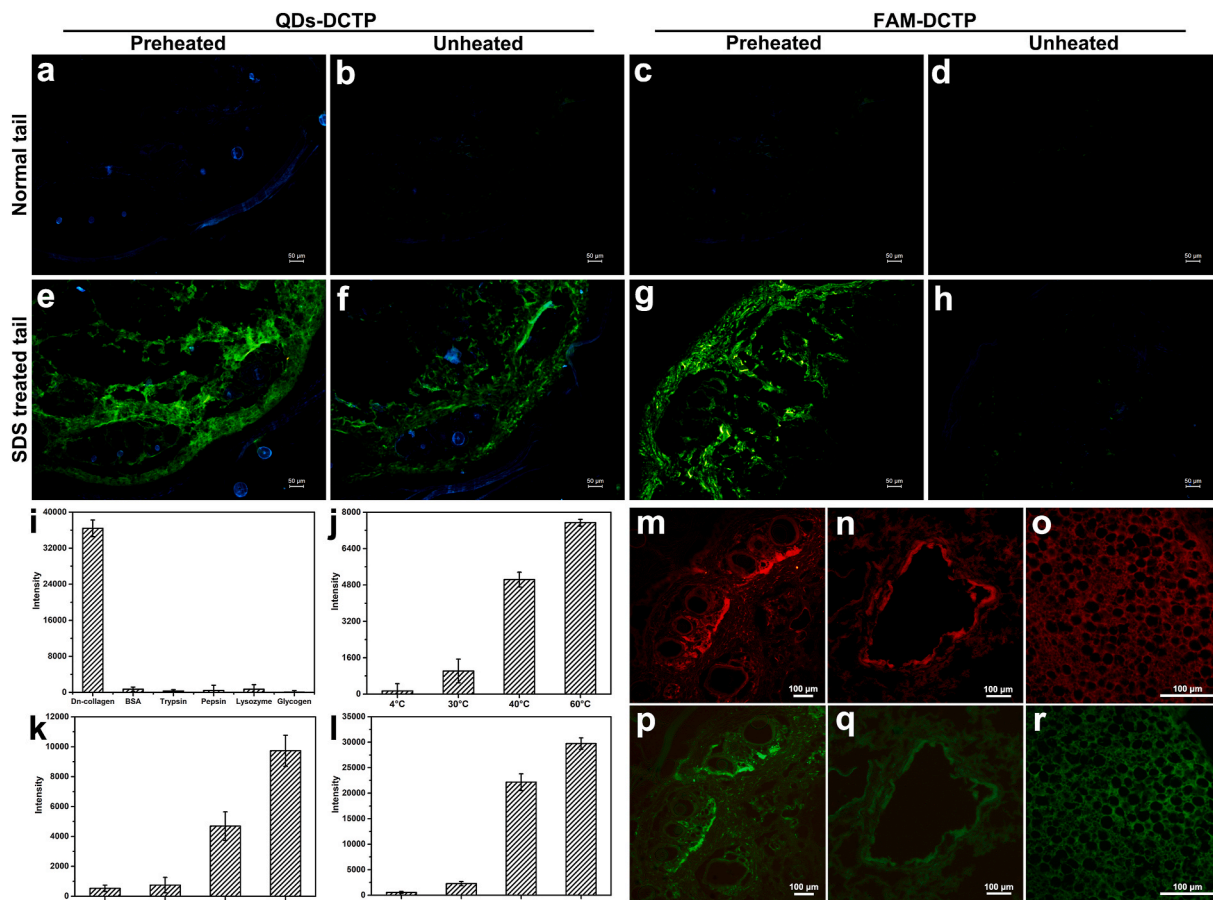

Fig. 2. Fluorescence micrographs of normal tail tissues stained with preheated DCTP-QDs (a), unheated DCTP-QDs (b), preheated DCTP-FAM (c), and unheated DCTP-FAM (d). Fluorescence micrographs of SDS-treated tail tissues stained with preheated DCTP-QDs (e), unheated DCTP-QDs (f), preheated DCTP-FAM (g), and unheated DCTP-FAM (h). Scale bar = 50 μm. Fluorescence intensity of DCTP-QDs binding to the wells coated with denatured collagen, BSA, trypsin, pepsin, lysozyme, and glycogen (i). Fluorescence intensity of DCTP-QDs binding to the wells coated with collagen pretreated by heating (j), UV irradiation (k) and SDS (l). The fluorescence micrographs of tail tissues stained with ICTP-QDs (m) and anti-collagen I antibody (p); The fluorescence micrographs of lung tissues stained with IICTP-QDs (n) and anti-collagen II antibody (q); The fluorescence micrographs of kidney tissues stained with IVCTP-QDs (o) and anti-collagen IV antibody (r).

fluorescence intensities observed in the wells coated with collagen pre-treated by UV irradiation for different durations (0, 30, 60, and 90 min) were 500, 1000, 5000, and 10000, respectively, indicating a progressive increase in collagen denaturation with longer irradiation time (Fig. 2k). The fluorescence intensities observed in the wells coated with collagen pre-treated with water, 0.1% SDS, 1% SDS, and 2% SDS were 500, 2500, 22000, and 30000, respectively, suggesting that concentrations of SDS above 1% significantly contributed to collagen denaturation (Fig. 2l). The DCTP-QDs probe has demonstrated remarkable versatility in specifically and sensitively detecting denatured collagen under diverse conditions.

The specificity of ICTP-QDs, IICTP-QDs, and IVCTP-QDs probes for targeting type I, II, and IV collagen was examined using fluorescence microscopy. Concurrently, anti-collagen antibodies were also applied to the tissue samples. The fluorescence micrographs of mouse tail tissues stained with ICTP-QDs exhibited strong fluorescence, mirroring the distribution observed in tissues stained with anti-collagen I, confirming the high specificity of ICTP-QDs in targeting type I collagen in tail tissues (Fig. 2m and p). Similarly, the fluorescence micrographs of sternum tissues stained with IICTP-QDs showed strong fluorescence, aligning seamlessly with tissues stained using anti-collagen II, indicating their selective identification of type II collagen (Fig. 2n and q). Additionally, the fluorescence micrographs of kidney tissues stained with IVCTP-QDs

displayed strong fluorescence, congruent with the distribution seen in tissues stained with anti-collagen IV, indicating their specific targeting of type IV collagen (Fig. 2o and r). These findings highlighted the distinct staining capabilities of each CTP-QDs probe for their respective collagen types.

The specificity of ICTP-QDs, IICTP-QDs, and IVCTP-QDs probes was further evaluated by comparison with GSH-QDs using fluorescence microscopy (Fig. S5). The fluorescence micrographs of rat skin tissues stained with ICTP-QDs exhibited strong fluorescence, while minimal fluorescence was observed in tissues stained with GSH-QDs, confirming the high specificity of ICTP-QDs in targeting type I collagen in skin tissues (Figs. S5a and S5d). Similarly, the fluorescence micrographs of sternum tissues stained with IICTP-QDs showed strong fluorescence, while minimal fluorescence was observed with GSH-QDs, indicating their selective identification of type II collagen (Figs. S5b and S5e). Additionally, the fluorescence micrographs of kidney tissues stained with IVCTP-QDs displayed strong fluorescence, with minimal fluorescence observed with GSH-QDs, indicating their specific targeting of type IV collagen (Figs. S5c and S5f). These findings underscored the unique staining abilities of each CTP-QDs probe for their specific collagen types, originating from the collagen-targeting peptides.
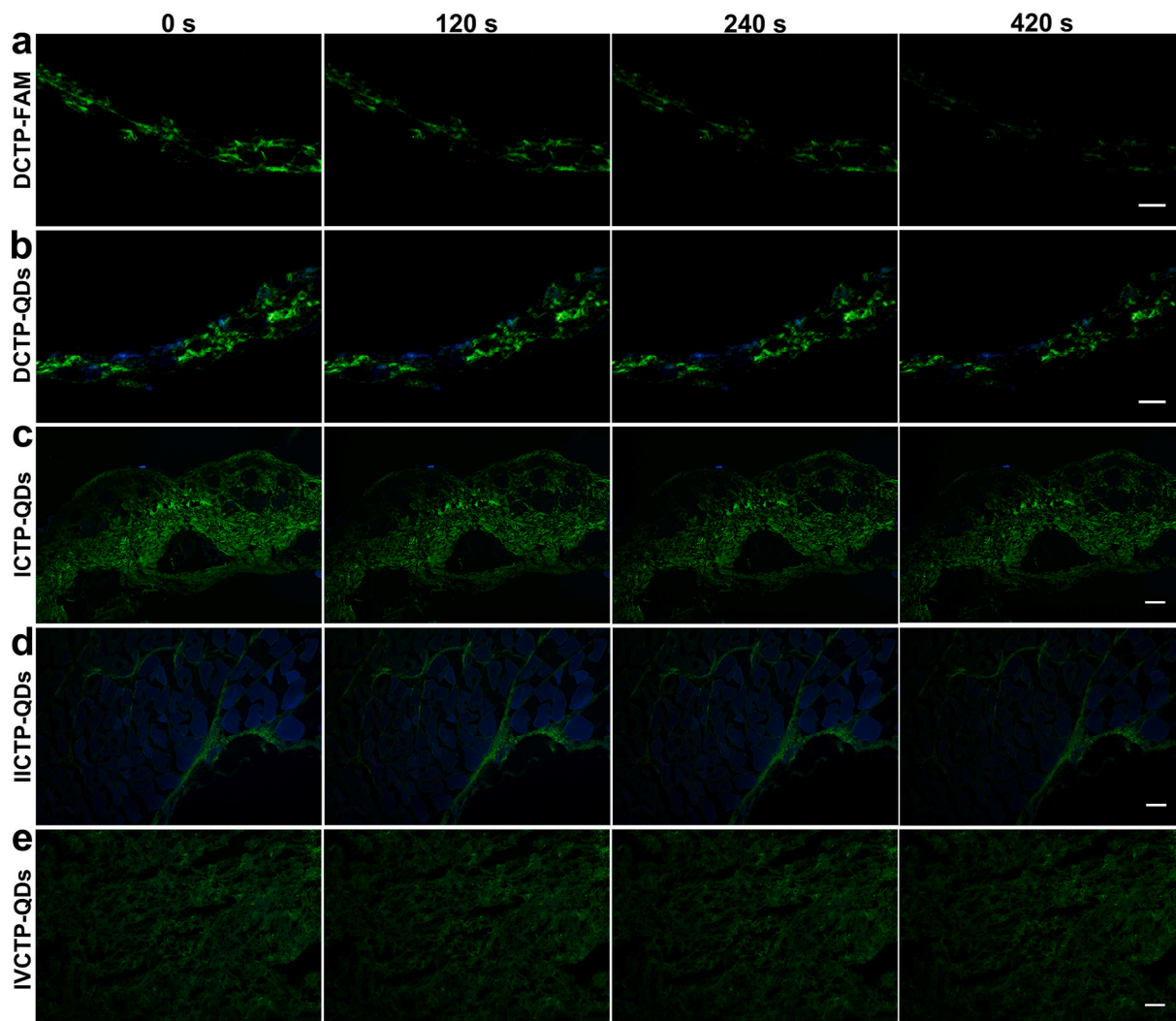

Fig. 3. Luminescence stability of CTP-QDs. a) Fluorescence micrographs of SDS-treated mice ear tissues staining using DCTP-FAM. b) Fluorescence micrographs of SDS-treated mice ear tissues staining using DCTP-QDs. c) Fluorescence micrographs of tail tissues staining using ICTP-QDs. d) Fluorescence micrographs of sternum tissues staining using IICTP-QDs. e) Fluorescence micrographs of kidney tissues staining using IVCTP-QDs. Scale bar = 50 μm.

3.4. Luminescence stability of the CTP-QDs probes

The luminescence stability of DCTP-QDs, ICTP-QDs, IICTP-QDs and IVCTP-QDs was assessed using fluorescence microscopy (Fig. 3). DCTP-QDs and DCTP-FAM probes were employed to stain SDS-treated ear tissues. The fluorescence micrographs of the ear tissues stained with the DCTP-FAM probe exhibited a pronounced reduction in fluorescence intensity over time during continuous ultraviolet irradiation. After 420 s of irradiation, the fluorescence signal from the DCTP-FAM probe became almost undetectable, indicating the rapid photobleaching of the probe (Fig. 3a). The quantitative analysis of fluorescence imaging area displayed a 90% reduction, which was consistent with disappearing fluorescence in fluorescence micrographs (Fig. S6a). In contrast, the fluorescence micrographs of ear tissues stained with the DCTP-QDs probe maintained strong green fluorescence even after 420 s of ultraviolet irradiation, highlighting the remarkable luminescence stability of DCTP-QDs (Fig. 3b). Moreover, the fluorescence micrographs of tail tissues stained with ICTP-QDs, sternum tissues stained with IICTP-QDs, and kidney tissues stained with IVCTP-QDs all exhibited persistent and intense green fluorescence even after 420 s of ultraviolet irradiation, confirming the exceptional luminescence stability of ICTP-QDs, IICTP-QDs, and IVCTP-QDs, respectively (Fig. 3c–e). The quantitative analysis of fluorescence imaging area showed only a reduction of less than 20% after continuous imaging for 120 s, and the fluorescence imaging area exhibited approximately a reduction of less than 40% after continuous imaging for 420 s, consistent with persistent fluorescence in micrographs (Figs. S6b–e). The luminescence stability of CTP-QDs probes significantly surpassed that of organic dye-labeled peptide probes, ensuring consistent and reliable signal intensity for accurate detection of multiple targets simultaneously.

The luminescence stability of the DCTP-QDs, ICTP-QDs, IICTP-QDs, and IVCTP-QDs probes was assessed over a pH range of 5.0–7.0 using fluorescence spectrometry (Fig. S6a). DCTP-FAM exhibited a substantial decrease in fluorescence intensity at pH 5.0 compared to pH 7.0, indicating its poor luminescence stability in acidic conditions and rendering it unsuitable for use in such environments. In contrast, DCTP-QDs exhibited consistent and high fluorescence intensity across the pH range of 5.0–7.0, indicating their remarkable luminescence stability. Similarly, the solutions of ICTP-QDs, IICTP-QDs, and IVCTP-QDs showed consistently high fluorescence intensities within the pH range of 5.0–7.0, further confirming the exceptional luminescence stability of CTP-QDs in both mildly acidic and neutral conditions.

The staining efficacy of CTP-QDs was further examined using fluorescence microscopy at pH 5.0 and 7.0 (Fig. S6b). The fluorescence micrographs of tail tissues stained with DCTP-FAM at pH 5.0 displayed significantly weaker green fluorescence compared to pH 7.0, indicating its limited efficacy in targeting denatured collagen at pH 5.0. In contrast, the fluorescence micrographs of tail tissues stained with DCTP-QDs at both pH 7.0 and pH 5.0 exhibited strong green fluorescence, demonstrating the robust staining capacity of DCTP-QDs even in acidic conditions. Similarly, the fluorescence micrographs of tail tissues stained with ICTP-QDs, sternum tissues stained with IICTP-QDs, and kidney tissues stained with IVCTP-QDs at both pH 7.0 and pH 5.0 displayed strong green fluorescence, confirming the excellent staining capabilities of CTP-QDs in both mildly acidic and neutral conditions. The mildly acidic environment (pH 5.0–7.0) is a prominent characteristic of numerous critical diseases, and the exceptional luminescence stability of CTP-QDs makes them an effective tool for detecting various collagen biomarkers in these diseased conditions.

3.5. Multicolor CTP-QDs probes for imaging connective tissues

The as-synthesized multicolor CTP-QDs probes were employed for imaging various collagen biomarkers in different types of connective tissues (Fig. 4). Fluorescence imaging of bladder tissues using multicolor DCTP probes with emission wavelengths of 525 nm, 580 nm, and 650 nm revealed distinct profiles of denatured collagen, visualized as green, orange, and red fluorescence signals respectively, highlighting the specificity of the probes in detecting collagen changes in SDS-treated bladder tissues (Fig. 4a–c). Multicolor imaging of tail tissues using
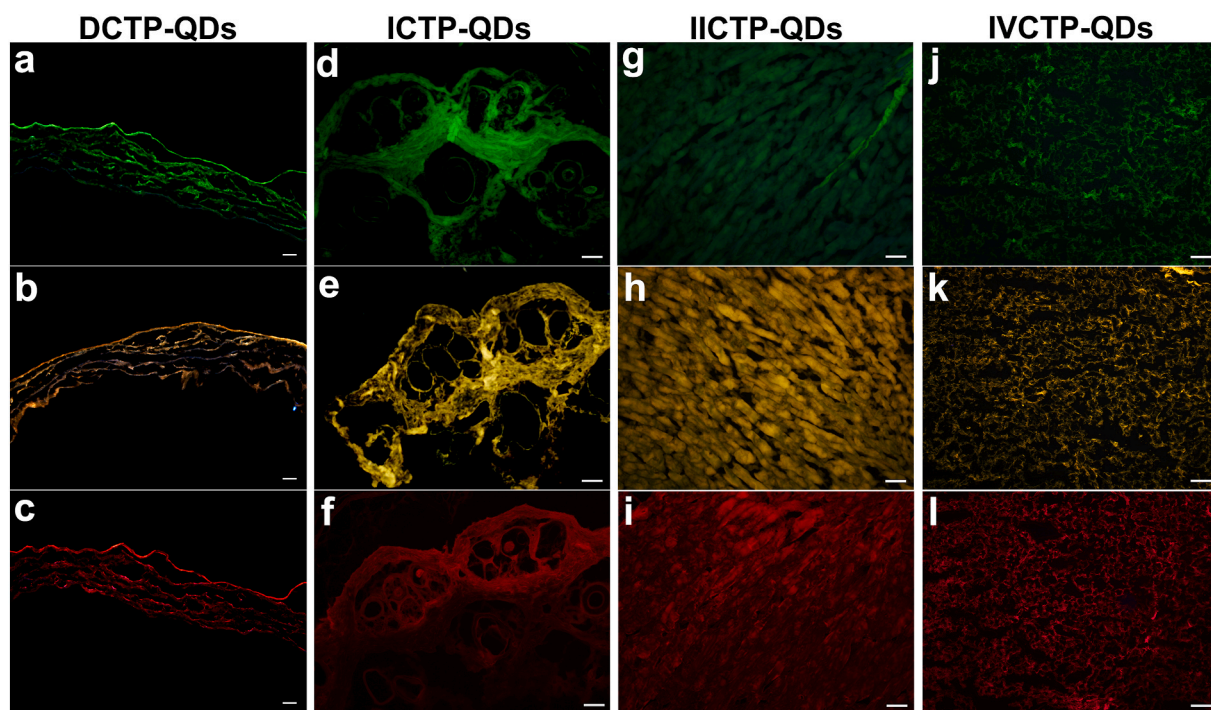

Fig. 4. Multi-color imaging of diverse connective tissues using CTP-QDs probes. Fluorescence micrographs of mice bladder tissues stained with green (a), orange (b) and red (c) DCTP-QDs; Fluorescence micrographs of mice tail tissues stained with green (d), orange (e) and red (f) ICTP-QDs; Fluorescence micrographs of sternum tissues stained with green (g), orange (h) and red (i) IICTP-QDs; Fluorescence micrographs of kidney tissues stained with green (j), orange (k) and red (l) IVCTP-QDs. Scale bar = 50 μm.

ICTP probes revealed specific staining patterns of type I collagen in tail tissues, depicted as green, orange, and red fluorescence signals respectively (Fig. 4d–f). Moreover, the utilization of multicolor IICTP-QDs and IVCTP-QDs probes for staining rat sternum and kidney tissues, respectively, resulted in micrographs showing green, orange, and red fluorescence, highlighting the remarkable selectivity of these probes for recognizing type II and type IV collagen (Fig. 4g-l). The multi-color CTP-QDs probes exhibited exceptional selectivity in detecting their respective targeted collagen biomarkers, offering a versatile toolkit for comprehensive fingerprinting of collagen profiles in various tissues.

3.6. Multiplex collagen fingerprinting in connective tissues using multicolor CTP-QDs probes

The multicolor CTP-QDs probes were employed for the fingerprinting of multiplex collagen biomarkers in diverse connective tissues affected by injuries (Fig. 5a–b). Green DCTP-QDs and red ICTP-QDs probes were employed for the co-staining of scalded skin tissues, resulting in fluorescence micrographs that exhibited intense green and red fluorescence signals, providing clear visualization of the simultaneous distribution of denatured collagen and type I collagen in the injured skin tissues (Fig. 5a). Green DCTP-QDs and red IICTP-QDs probes were utilized for the co-staining of heat-damaged ear tissue, and the resulting fluorescence micrograph displayed strong green and red fluorescence signals, enabling simultaneous visualization of the distribution of denatured collagen and type II collagen in the injured ear tissues (Fig. 5b).

The multicolor CTP-QDs probes were applied to fingerprint multiplex collagen biomarkers in connective tissues impacted by severe diseases such as tumors and fibrosis (Fig. 5c–d). Green DCTP-QDs and red IVCTP-QDs probes were employed to simultaneously stain breast cancer tissues, revealing abundant overlapping green and red fluorescence signals in the fluorescence micrographs, which effectively depict the disruption and remodeling of type IV collagen structure during tumor progression (Fig. 5c). It is noteworthy that tissues stained with CTP-QDs probes did not exhibit significant autofluorescence, which is a common background signal in simultaneous QDs imaging [44,45]. Moreover, green ICTP-QDs and red IVCTP-QDs probes were employed for the co-staining of liver fibrosis tissue. The resulting fluorescence micrograph revealed intense red and green fluorescence signals, allowing for the visualization of the distribution of interstitium and basement membrane in the fibrotic liver tissue (Fig. 5d).

The multicolor CTP-QDs probes were further employed to profile multiplex collagen biomarkers during bone development (Fig. 5e). Green DCTP-QDs and red ICTP-QDs were used for staining tissues throughout the whole mouse embryo. The fluorescence micrographs revealed a uniform distribution of type I collagen throughout the embryo, whereas denatured collagen was predominantly localized in developing bone tissues such as vertebrae. It offered a comprehensive and high-resolution depiction of collagen dynamics and organization during bone formation, capturing the synthesis of type I collagen and the degradation of fibrillar collagen, thus providing valuable insights into the intricate processes involved in bone remodeling. The multicolor CTP-QDs probes served as a highly robust tool for the multiplex fingerprinting of collagen in various types of connective tissues, whether affected by injury, disease, or undergoing remodeling processes.

4. Conclusion

The simultaneous fingerprinting of multiplex collagen biomarkers is of paramount importance in the diagnosis and treatment of various severe diseases, such as tumors and fibrosis. QDs have attracted significant interest in the field of multiplex biological imaging due to their exceptional photostability, vibrant color emission, and wide excitation spectra. The current approaches for achieving hydrophilic QDs often involve additional post-modification steps, which significantly impact the stability and specificity of the resulting peptide-QDs probes.

We report for the first time the creation of multi-color QDs-based peptide probes for simultaneous fingerprinting of multiplex collagen biomarkers in connective tissues. Using a bipeptide system composed of GSH as the host peptide and a collagen-targeting peptide as the guest peptide, we have developed highly stable hydrophilic QDs-based probes with a coordinative Cys residue for QDs connection and a negatively charged Glu residue for electrostatic repulsion-based QDs stabilization. The high thermal stability of CTPs allows for their direct addition at the beginning of high-temperature reactions, facilitating the one-pot
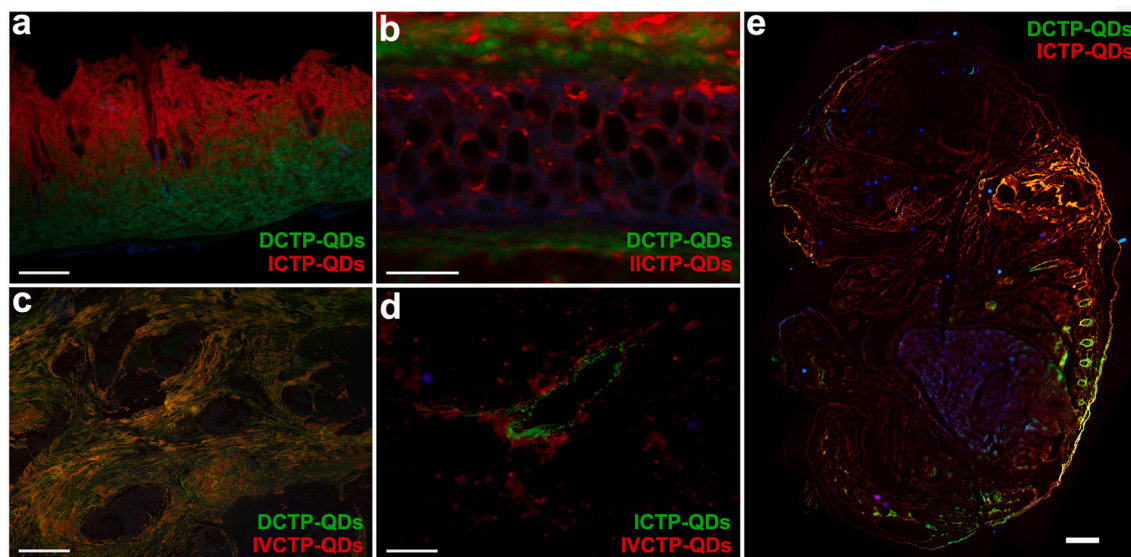

Fig. 5. Multiplex collagen fingerprinting in connective tissues using multicolor CTP-QDs probes. (a) Fluorescence micrographs of scalded rat skin tissue co-stained with DCTP-QDs and ICTP-QDs. Scale bar = 100 μm. (b) Fluorescence micrographs of damaged rat ear tissue co-stained with DCTP-QDs and IICTP-QDs. Scale bar = 100 μm. (c) Fluorescence micrographs of breast cancer tissue co-stained with DCTP-QDs and IVCTP-QDs. Scale bar = 100 μm. (d) Fluorescence micrographs of liver fibrosis tissue co-stained with ICTP-QDs and IVCTP-QDs. Scale bar = 100 μm. (e) Fluorescence micrographs of mice embryo co-stained with DCTP-QDs and ICTP-QDs. Scale bar = 2000 μm.

synthesis of specific hydrophilic QDs without requiring additional secondary modifications.

The bipeptide system has proven to be a versatile tool for the facile production of high-quality multicolor CTP-QDs, offering flexibility through simple adjustment of incubation time and incorporation of targeting peptides specific to different collagen types. Four CTP-QDs probes have been synthesized as examples, demonstrating superior specificity in targeting important collagen biomarkers such as denatured collagen, type I collagen, type II collagen, and type IV collagen. Notably, the larger size of QDs nanoparticles compared to FAM effectively disrupts the triple helix conformation of DCTP without compromising its binding affinity, facilitating the specific and sensitive detection of denatured collagen using DCTP-QDs under diverse conditions without the need of potentially harmful preheating treatment required for DCTP-FAM.

In contrast to organic dye-labeled peptide probes with rapid photobleaching and high susceptibility to environmental factors, the CTP-QDs probes exhibit remarkable luminescence stability during long ultraviolet irradiation and in both mildly acidic and neutral conditions, enabling consistent and reliable signal intensity for accurate simultaneous detection of multiple collagen biomarkers in diseased conditions characterized by a mildly acidic environment. The multicolor CTP-QDs probes have demonstrated great efficacy in simultaneously fingerprinting multiple collagen types in diverse connective tissues, regardless of their status, whether affected by injury, disease, or undergoing remodeling processes. The innovative multicolor CTP-QDs probes offer a powerful toolkit for the multiplex fingerprinting of collagen, presenting great potential in the diagnosis and management of collagen-related diseases such as tumors and fibrosis.

CRediT authorship contribution statement

Xiangdong Cai: Writing – original draft, Visualization, Methodology, Formal analysis, Data curation. **Bo Wang:** Visualization, Methodology, Formal analysis, Data curation. **Linge Nian:** Resources. **Tao Cheng:** Methodology. **Chunxia Zhang:** Formal analysis, Investigation. **Lu Li:** Formal analysis, Investigation. **Guangrui Zhang:** Methodology, Resources. **Jianxi Xiao:** Writing – review & editing, Supervision, Funding acquisition, Conceptualization, Project administration, Resources, Writing – original draft.

Declaration of competing interest

The authors declare the following financial interests/personal relationships which may be considered as potential competing interests: Jianxi Xiao reports was provided by National Natural Science Foundation of China. Jianxi Xiao reports was provided by Natural Science Foundation of Gansu Province. Xiangdong Cai reports was provided by China Postdoctoral Science Foundation.

Data availability

Data will be made available on request.

Appendix B. Supplementary data

Supplementary data to this article can be found online at https://doi.org/10.1016/j.mtbio.2024.101026.

References

[1] K. Gelse, E. Poschl, T. Aigner, Collagens - structure, function, and biosynthesis, Adv. Drug Deliv. Rev. 55 (12) (2003) 1531–1546, https://doi.org/10.1016/j.addr.2003.08.002.
[2] D.J. Prockop, K.I. Kivirikko, Collagens - molecular-biology, diseases, and potentials for therapy, Annu. Rev. Biochem. 64 (1995) 403–434, https://doi.org/10.1146/annurev.biochem.64.1.403.
[3] A. Sorushanova, L.M. Delgado, Z.N. Wu, N. Shologu, A. Kshirsagar, R. Raghunath, A.M. Mullen, Y. Bayon, A. Pandit, M. Raghunath, D.I. Zeugolis, The collagen suprafamily: from biosynthesis to advanced biomaterial development, Adv. Mater. 31 (1) (2019). Artn180165110.1002/Adma.201801651.
[4] C. Bonnans, J. Chou, Z. Werb, Remodelling the extracellular matrix in development and disease, Nat. Rev. Mol. Cell Biol. 15 (12) (2014) 786–801, https://doi.org/10.1038/nrm3904.
[5] J.J. Tomasek, G. Gabbiani, B. Hinz, C. Chaponnier, R.A. Brown, Myofibroblasts and mechano-regulation of connective tissue remodelling, Nat. Rev. Mol. Cell Biol. 3 (5) (2002) 349–363, https://doi.org/10.1038/nrm809.
[6] M. Fang, J.P. Yuan, C.W. Peng, Y. Li, Collagen as a double-edged sword in tumor progression, Tumor Biol. 35 (4) (2014) 2871–2882, https://doi.org/10.1007/s13277-013-1511-7.
[7] T.A. Wynn, Common and unique mechanisms regulate fibrosis in various fibroproliferative diseases, J. Clin. Invest. 117 (3) (2007) 524–529, https://doi.org/10.1172/JCI31487.
[8] T.E. King, M.I. Schwarz, K. Brown, J.A. Tooze, T.V. Colby, J.A. Waldron, A. Flint, W. Thurlbeck, R.M. Cherniack, Idiopathic pulmonary fibrosis - relationship between histopathologic features and mortality, Am J Resp Crit Care 164 (6) (2001) 1025–1032, https://doi.org/10.1164/ajrccm.164.6.2001056.
[9] G. Germani, A.K. Burroughs, A.P. Dhillon, The relationship between liver disease stage and liver fibrosis: a tangled web, Histopathology 57 (6) (2010) 773–784, https://doi.org/10.1111/j.1365-2559.2010.03609.x.
[10] R. Kalluri, Basement membranes: structure, assembly and role in tumour angiogenesis, Nat. Rev. Cancer 3 (6) (2003) 422–433, https://doi.org/10.1038/nrc1094.
[11] M.A. Shields, S. Dangi-Garimella, A.J. Redig, H.G. Munshi, Biochemical role of the collagen-rich tumour microenvironment in pancreatic cancer progression, Biochem. J. 441 (2012) 541–552, https://doi.org/10.1042/Bj20111240.
[12] B. Emon, J. Bauer, Y. Jain, B. Jung, T. Saif, Biophysics of tumor microenvironment and cancer metastasis - a mini review, Comput Struct Biotec 16 (2018) 279–287, https://doi.org/10.1016/j.csbj.2018.07.003.
[13] K. Wang, F. Wu, B.R. Seo, C. Fischbach, W.S. Chen, L. Hsu, D. Gourdon, Breast cancer cells alter the dynamics of stromal fibronectin-collagen interactions, Matrix Biol. 60–61 (2017) 86–95, https://doi.org/10.1016/j.matbio.2016.08.001.
[14] M. Jovic, I. Nikolic, V. Todorovic, A. Petrovic, V. Petrovic, M. Mojsilovic, T. Dencic, Distribution of collagen I, III, and IV and laminin in the human liver during prenatal development, Cells Tissues Organs 205 (3) (2018) 164–177, https://doi.org/10.1159/000489476.
[15] K.M. Mak, E. Chu, K.H.V. Lau, A.J. Kwong, Liver fibrosis in elderly cadavers: localization of collagen types I, III, and IV, alpha-smooth muscle actin, and elastic fibers, Anat. Rec. 295 (7) (2012) 1159–1167, https://doi.org/10.1002/ar.22504.
[16] S. Duarte, J. Saber, T. Fujii, A.J. Coito, Matrix metalloproteinases in liver injury, repair and fibrosis, Matrix Biol. 44–46 (2015) 147–156, https://doi.org/10.1016/j.matbio.2015.01.004.
[17] K.M. Mak, R. Mei, Basement membrane type IV collagen and laminin: an overview of their biology and value as fibrosis biomarkers of liver disease, Anat. Rec. 300 (8) (2017) 1371–1390, https://doi.org/10.1002/ar.23567.
[18] X.B. Yao, F. Cheng, W.M. Yu, T. Rao, W. Li, S. Zhao, X.J. Zhou, J.Z. Ning, Kidney fibrosis induced by various irrigation pressures in mouse models of mild and severe hydronephrosis, Int. Urol. Nephrol. 51 (2) (2019) 215–222, https://doi.org/10.1007/s11255-018-2040-5.
[19] K.A. Elsaid, C.O. Chichester, Review: collagen markers in early arthritic diseases, Clin. Chim. Acta 365 (1–2) (2006) 68–77, https://doi.org/10.1016/j.cca.2005.09.020.
[20] S.R. Goldring, M.B. Goldring, Changes in the osteochondral unit during osteoarthritis: structure, function and cartilage-bone crosstalk, Nat. Rev. Rheumatol. 12 (11) (2016) 632–644, https://doi.org/10.1038/nrrheum.2016.148.
[21] J. Hwang, Y.F. Huang, T.J. Burwell, N.C. Peterson, J. Connor, S.J. Weiss, S.M. Yu, Y. Li, In situ imaging of tissue remodeling with collagen hybridizing peptides, ACS Nano 11 (10) (2017) 9825–9835, https://doi.org/10.1021/acsnano.7b03150.
[22] Y. Li, C.A. Foss, D.D. Summerfield, J.J. Doyle, C.M. Torok, H.C. Dietz, M. G. Pomper, S.M. Yu, Targeting collagen strands by photo-triggered triple-helix hybridization, P Natl Acad Sci USA 109 (37) (2012) 14767–14772, https://doi.org/10.1073/pnas.1209721109.
[23] Y. Li, D. Ho, H. Meng, T.R. Chan, B. An, H. Yu, B. Brodsky, A.S. Jun, S.M. Yu, Direct detection of collagenous proteins by fluorescently labeled collagen mimetic peptides, Bioconjugate Chem. 24 (1) (2013) 9–16, https://doi.org/10.1021/bc3005842.
[24] W. Chen, H. Yu, Y. Hao, W. Liu, R. Wang, Y. Huang, J. Wu, L. Feng, Y. Guan, L. Huang, K. Qian, Comprehensive metabolic fingerprints characterize neuromyelitis optica spectrum disorder by nanoparticle-enhanced laser desorption/ionization mass spectrometry, ACS Nano 17 (20) (2023) 19779–19792, https://doi.org/10.1021/acsnano.3c03765.
[25] D. Liang, Y. Wang, K. Qian, Nanozymes: applications in clinical biomarker detection, Interdisciplinary Medicine 1 (4) (2023), https://doi.org/10.1002/inmd.20230020.

[26] F. Zhu, S. Liu, X. Bai, X. Liu, B. Lin, Y. Lu, Point-of-care multiplexed single-cell protein secretion analysis based on tyramide signal amplification, View 4 (1) (2022), https://doi.org/10.1002/viw.20220033.

[27] X.D. Cai, Z. Liu, S. Zhao, C. Song, S.L. Dong, J.X. Xiao, A single stranded fluorescent peptide probe for targeting collagen in connective tissues, Chem. Commun. 53 (87) (2017) 11905–11908, https://doi.org/10.1039/c7cc06056d.

[28] M. Baues, B.M. Klinkhammer, J. Ehling, F. Gremse, M.A.M.J. van Zandvoort, C.P. M. Reutelingsperger, C. Daniel, K. Amann, J. Babickova, F. Kiessling, J. Floege, T. Lammers, P. Boor, A collagen-binding protein enables molecular imaging of kidney fibrosis in vivo, Kidney Int. 97 (3) (2020) 609–614, https://doi.org/10.1016/j.kint.2019.08.029.

[29] B.A. Helms, S.W.A. Reulen, S. Nijhuis, P.T.H.M. de Graaf-Heuvelmans, M. Merkx, E.W. Meijer, High-affinity peptide-based collagen targeting using synthetic phage mimics: from phage display to dendrimer display, J. Am. Chem. Soc. 131 (33) (2009) 11683, https://doi.org/10.1021/ja902285m.

[30] J.M. Chan, L.F. Zhang, R. Tong, D. Ghosh, W.W. Gao, G. Liao, K.P. Yuet, D. Gray, J. W. Rhee, J.J. Cheng, G. Golomb, P. Libby, R. Langer, O.C. Farokhzad, Spatiotemporal controlled delivery of nanoparticles to injured vasculature, P Natl Acad Sci USA 107 (5) (2010) 2213–2218, https://doi.org/10.1073/pnas.0914585107.

[31] H.Y. Hu, N.H. Lim, D. Ding-Pfennigdorff, J. Saas, K.U. Wendt, O. Ritzeler, H. Nagase, O. Plettenburg, C. Schultz, M. Nazare, DOTAM derivatives as active cartilage-targeting drug carriers for the treatment of osteoarthritis, Bioconjugate Chem. 26 (3) (2015) 383–388, https://doi.org/10.1021/bc500557s.

[32] A.Y. Wang, X. Mo, C.S. Chen, S.M. Yu, Facile modification of collagen directed by collagen mimetic peptides, J. Am. Chem. Soc. 127 (12) (2005) 4130–4131, https://doi.org/10.1021/Ja0431915.

[33] A.Y. Wang, C.A. Foss, S. Leong, X. Mo, M.G. Pomper, S.M. Yu, Spatio-temporal modification of collagen scaffolds mediated by triple helical propensity, Biomacromolecules 9 (7) (2008) 1755–1763, https://doi.org/10.1021/bm701378k.

[34] X.D. Cai, W.Y. Wei, Y.H. Bi, Z. Liu, Z.T. Bai, J.Q. Lei, J.X. Xiao, An intrinsically nontrimerizing peptide probe for specifically targeting pathological collagen in connective tissues, Adv. Funct. Mater. 30 (42) (2020). Artn200453210.1002/Adfm.202004532.

[35] J.L. Santos, Y. Li, H.R. Culver, M.S. Yu, M. Herrera-Alonso, Conducting polymer nanoparticles decorated with collagen mimetic peptides for collagen targeting, Chem. Commun. 50 (95) (2014) 15045–15048, https://doi.org/10.1039/c4cc06056c.

[36] M. Alizadeh-Ghodsi, M. Pourhassan-Moghaddam, A. Zavari-Nematabad, B. Walker, N. Annabi, A. Akbarzadeh, State-of-the-Art and trends in synthesis, properties, and application of quantum dots-based nanomaterials, Part. Part. Syst. Char. 36 (2) (2019). Artn180030210.1002/Ppsc.201800302.

[37] K.D. Wegner, N. Hildebrandt, Quantum dots: bright and versatile in vitro and in vivo fluorescence imaging biosensors, Chem. Soc. Rev. 44 (14) (2015) 4792–4834, https://doi.org/10.1039/c4cs00532e.

[38] W.B. Cai, X.Y. Chen, Preparation of peptide-conjugated quantum dots for tumor vasculature-targeted imaging, Nat. Protoc. 3 (1) (2008) 89–96, https://doi.org/10.1038/nprot.2007.478.

[39] M. Michalska, A. Florczak, H. Dams-Kozlowska, J. Gapinski, S. Jurga, R. Schneider, Peptide-functionalized ZCIS QDs as fluorescent nanoprobe for targeted HER2-positive breast cancer cells imaging, Acta Biomater. 35 (2016) 293–304, https://doi.org/10.1016/j.actbio.2016.02.002.

[40] Y.G. Zheng, S.J. Gao, J.Y. Ying, Synthesis and cell-imaging applications of glutathione-capped CdTe quantum dots, Adv. Mater. 19 (3) (2007) 376, https://doi.org/10.1002/adma.200600342.

[41] B.R. Liu, J.F. Li, S.W. Lu, H.J. Lee, Y.W. Huang, K.B. Shannon, R.S. Aronstam, Cellular internalization of quantum dots noncovalently conjugated with arginine-rich cell-penetrating peptides, J. Nanosci. Nanotechnol. 10 (10) (2010) 6534–6543, https://doi.org/10.1166/jnn.2010.2637.

[42] B.R. Liu, Y.W. Huang, J.G. Winiarz, H.J. Chiang, H.J. Lee, Intracellular delivery of quantum dots mediated by a histidine- and arginine-rich HR9 cell-penetrating peptide through the direct membrane translocation mechanism, Biomaterials 32 (13) (2011) 3520–3537, https://doi.org/10.1016/j.biomaterials.2011.01.041.

[43] J. Brunetti, G. Riolo, M. Gentile, A. Bernini, E. Paccagnini, C. Falciani, L. Lozzi, S. Scali, L. Depau, A. Pini, P. Lupetti, L. Bracci, Near-infrared quantum dots labelled with a tumor selective tetrabranched peptide for in vivo imaging, J. Nanobiotechnol. 16 (2018). ARTN2110.1186/s12951-018-0346-1.

[44] X.L. Liu, C.W. Peng, C. Chen, X.Q. Yang, M.B. Hu, H.S. Xia, S.P. Liu, D.W. Pang, Y. Li, Quantum dots-based double-color imaging of HER2 positive breast cancer invasion, Biochem. Biophys. Res. Commun. 409 (3) (2011) 577–582, https://doi.org/10.1016/j.bbrc.2011.05.052.

[45] C.W. Peng, X.L. Liu, C. Chen, X. Liu, X.Q. Yang, D.W. Pang, X.B. Zhu, Y. Li, Patterns of cancer invasion revealed by QDs-based quantitative multiplexed imaging of tumor microenvironment, Biomaterials 32 (11) (2011) 2907–2917, https://doi.org/10.1016/j.biomaterials.2010.12.053.